RESEARCH ARTICLE

INTERNATIONAL RESEARCH JOURNAL OF MULTIDISCIPLINARY TECHNOVATION

Asian Research Association

DOI: 10.54392/irjmt24211

Radiology Image Data Augmentation and Image Enhancement in Respiratory Disease Infection Detection Using Machine Learning Approach

Prita Patil [a,*], Vaibhav Narawade [a]

[a] Department of Computer Engineering, Ramrao Adik Institute of Technology, DY Patil Deemed to be University, Navi Mumbai, Maharashtra 400706, India.

* Corresponding Author Email: prita.patil@dypatil.edu

DOI: https://doi.org/10.54392/irjmt24211

Received: 08-12-2023; Revised: 23-02-2024; Accepted: 05-03-2024; Published: 12-03-2024

Abstract: Medical imaging plays an important role in medical diagnosis and treatment. It is also useful in medical applications. The proposed concept's goal is to understand the importance of data balancing, data augmentation, and segmentation in the clinical field, to improve image data balancing using data augmentation and edge detection techniques, to improve radiology image preprocessing to locate regions of interest (ROI), and to construct custom-built Deep Neural Networks (DNN) in diagnosing respiratory illness using Machine Learning approaches. Images of varying quality from multiple machine types are frequently included in different datasets. This study used four datasets, three of which are online datasets from Kaggle and the fourth is real-time radiology pictures of COVID and Pneumonia-infected persons from neighboring local hospitals. We proposed RESP_DATA_BALANCE for image data balance in dataset construction, and RDD_ROI (Respiratory Disease Detection Region of Interest) algorithm, which combines improved image feature extraction technique using a GLCM and unsupervised K-means clustering for segmentation to identify the region of interest in the detection of respiratory diseases. Our suggested custom-built 28-layer Respiratory Disease Detection Deep Neural Network (RDD_DNN) is used for further training, testing, and validation. Furthermore, experimental results focus on performance characteristics using various data augmentation, edge detection, and preprocessing strategies. The experimental purpose of our research study is to aid in the classification and early diagnosis of respiratory disorders.

Keywords: Medical imaging data, Radiology images, Respiratory disease, COVID-19, Data Augmentation, Segmentation

1. Introduction

Lung trouble is another name for a respiratory ailment. The essential point is that this condition may be identified, and evaluated in various patterns, and forms of lung disease. Pneumonia, COVID-19, and TB are the most common types of lung illness. The primary issue in many nations with this condition is a shortage of radiologists [1]. DL (Deep Learning) and ML (Machine Learning) may be used to classify, identify, and quantify medical pictures [2]. CXR (Chest X-ray) pictures and chest radiography are processed for the respiratory illness medical imaging system. Machine learning approaches are setting new criteria in the field of medical pictures and detecting respiratory illness. Many big chest radiographs are used in the computer assistance diagnostic for respiratory illness [3]. ML techniques for medical image application for respiratory disease detection have reached tremendous heights. In lung disease, interstitial infiltrate changes are very predictive and limited [4]. Moreover, examining different machine learning with image processing and classification is based on several attributes [5, 6]. The medical images dataset has different perspectives and uses CAD with machine learning algorithms the existing scholars have chest x-ray images to deliver significant knowledge regarding COVID-19 from CXR images, which should come from every remote location in different countries. If we talk about COVID-19, symptoms are cough, fatigue, and fever. On the other hand, diarrhea and sputum for excess [7]. In multiple cases, pneumonia leads to deprivation of oxygen.

Many Image categorization is a prominent research topic in the science of computer vision. Despite the fact that the emergence of deep learning technology has accelerated the development of the image field, with the continuous breakthrough of deep learning in the field of computer vision, the deep neural network has improved various image recognition evaluation indicators with its powerful learning ability [8]. However, diverse picture datasets in the enormous data have their

own unique difficulties that restrict their identification ability. Furthermore, the imbalance problem in picture classification tasks is highly widespread in real-world applications and has emerged as a major issue in the fields of machine learning and data mining [9]. The classification network directs training based on the training set samples and then classifies the test samples using the trained classification network [10].

The categorization of imbalanced high-dimensional picture data remains a big issue, especially with relatively small samples of some minority classes [11]. It is worth mentioning that many real-world data are prone to the phenomena of category imbalance, which occurs when the quantity of samples in various categories is substantially varied. This is known as the imbalance problem, and it has long plagued academics and industry. There is an issue. In a class-imbalanced dataset, the dominant class has more samples than the minority class. A number of outstanding classification algorithms have arisen as a consequence of the efforts of numerous researchers, and some practical results have been obtained. However, the vast majority of the current existing classification methods perform poorly when the training dataset displays an imbalanced distribution; they are primarily intended for datasets with balanced class distributions. Thus, it is a cormance is maintained while simultaneously improving the minority hallenging task to ensure that the majority class's classification perfclass's classification performance in these unbalanced classification tasks [12].

Extraneous characteristics or picture areas reduce the model's performance; hence, it is critical to train a model with only the most significant features. As a result, the most critical step prior to the training stage is establishing the Region of Interest (ROI). For this reason, segmentation is useful since it may separate the irrelevant and unneeded elements of an image. There is a variety of open-source automatic segmentation methods available, including region-based, edge-based, clustering, and so on. Unnecessary features or image areas detract from the model's performance. As a result, the most critical step prior to the training stage is establishing the Region of Interest (ROI). For this reason, segmentation is useful since it may separate the irrelevant and unneeded elements of an image.A large amount of modern medical data is represented by images or other types of digital signals, such as X-rays, MRI, computer tomography (CT), positron emission tomography, single-photon emission computed tomography, electrical impedance tomography, and ultrasound [13, 14]. Massive volumes of sophisticated picture data have resulted in the development of automated medical image processing and analysis. The editing and analysis of images produced by discretizing continuous signals is the focus of digital image processing [15, 16].

Medical imaging segmentation is important for obtaining information about the status of various tissues, organs, and Medical imaging segmentation is critical for determining the state of various tissues, organs, and other bodily parts [17]. The segmentation accuracy and decision confidence value of any lung analysis system for spotting anomalies are strongly reliant on an appropriate lung segmentation technique. As a result, lung images are critical to the performance of segmentation-based algorithms. Due to poor image contrast and artifacts that result in missing or diffuse organ/tissue borders, medical image segmentation is problematic. As a result, this task necessitates the incorporation of as much prior information as possible, such as texture, shape, organ spatial position, and so on. Manual segmentation is not only time intensive and tedious, but it is also prone to error. Expert segmentation has been discovered to be effective. Expert segmentation has been observed to vary by up to 20% [18]. As a result, numerous automatic and semiautomatic procedures have been presented. Because most existing algorithms for segmenting medical images only work on a specific type of image, they have limitations. As a result, a method medical imaging becomes more important. The main advantage of using unsupervised segmentation over supervised segmentation is that it does not require tagged training data. This is an important factor to consider in medical imaging and related applications [19].

The novel contribution of this work is outlined as follows:

- Extraction and interpretation of radiological pictures in the detection of respiratory disease
- Understanding the importance of data balancing, data augmentation and image enhancement using Machine Learning.
- Proposition of improved data balancing algorithm RESP_DATA_BALANCING using data augmentation
- Proposition of improvement in image enhancement and preprocessing of radiology images in the detection of respiratory diseases with RDD_ROI algorithm
- Proposition of Custom Built Deep Neural Network model in the detection of respiratory diseases.
- Comparative performance analysis and experimental evaluation of classification models to understand the effectiveness of image data balancing data augmentation techniques, image data segmentation, and different respiratory datasets etc.

2. Related Work

The literature review focuses on principles and previous research work on data balance, data augmentation, ROI detection, segmentation, and so on.

2.1 Survey on different data balancing and data augmentation

One of the most significant difficulties encountered in the radiology pictures classification problem is the scarcity of images, making the datasets unbalanced. In this section, we have discussed different data balancing technique for classification

- Oversampling: Oversampling is the most commonly used method in multi-class imbalanced data preprocessing techniques, which solves the multi-class imbalance problem by introducing new minority class instances, thereby realizing the rebalancing of the original skewed data [20]. However, random copying of samples does not introduce new information, and excessive copying of minority class samples will generate a large number of repeated samples, making the network overfitting. Oversampling is the most commonly used method in multi-class imbalanced data preprocessing techniques.
- Undersampling : Undersampling, as opposed to oversampling, preserves class balance by limiting the quantity of samples from the dominant class [21]. The presence of a class overlap problem in multi-class imbalanced data will lead the classifier to fail to identify class borders efficiently, lowering the classifier's performance. Hartono presented the LOFCUS undersampling approach, which employs the LOF local outlier factor and boxplot to clean the noisy samples in the training data set and removes the samples that play a vital part in the classification based on the class overlap. Undersampling enhances classifier accuracy by increasing the retention of the original data distribution [22].
- Hybrid Sampling: The oversampling and undersampling algorithms each have advantages and downsides in the class unbalanced data preparation approach. To reduce data imbalance, some researchers combine the two types of sampling and process the majority and minority classes at the same time [23].

In [24], the author proposed SMOTE, a minority class sample synthesis approach. First, a minority class sample is chosen at random as the main sample, then the K nearest neighbor samples of the main sample are chosen from the remaining minority class samples, and finally, a minority class sample is chosen at random from the nearest neighbor samples, and the sample is randomly connected to the main sample. Sampling, and then using the obtained locations as synthetic minority class samples. However, due to the creation of incorrect samples, the minority class is over-generalized to the majority class region, impairing the learnability of minority class samples [24]. Wang Xiao devised SSCMIO, a synthetic minority oversampling approach based on k-nearest neighbors, to improve SMOTE. When processing data, the k-nearest neighbor direction of each instance is provided a selection weight, and the neighboring direction that may cause severe overgeneralization is given a lower selection weight. This method uses safer nearby directions to synthesize instances and employs NBDOS clustering to avoid calculating the selection weights of some minority class examples. Simultaneously, two-loop filtering is employed to reduce the calculation of the distance between a large number of instances [25]. SSCMIO also presents a strategy to avoid over-generalization, over-sampling based on the safety factor of instance neighborhoods, and assigns lower weights to regions that may cause over-generalization, which can effectively limit the incidence of class overlap.

Hartono presented LOFCUS, a class overlap-based undersampling approach that employs the LOF local outlier factor and boxplot to clean the noisy samples in the training data set and removes the samples that play a vital role in the classification based on the class overlap. Undersampling enhances classifier accuracy by maximizing the preservation of the original data distribution [26]. In imbalanced datasets, clustering algorithms paired with undersampling can efficiently manage majority classes. CUS is a clustering-based undersampling method suggested by Krawczyk. After clustering the majority of class instances, the instances with the most information are undersampled to generate numerous balanced datasets. Experiments show that this strategy is useful in classifying instances of the majority and minority classes, with high accuracy [27]. Arefeen uses multi-class unbalanced data that has been trained and balanced, and offers a two-stage OCSV-US [28] algorithm that combines undersampling and genetic algorithms. The first stage involves training M single-class classifiers based on the number of multi-classes, and each classifier returns a set of class instances with the highest informative value for sampling in the next stage. In the second stage, several random under sampled data subsets are produced based on the class instances from the previous phase, and the subsets are evolved using the genetic algorithm until their fitness function can no longer be improved. The most suitable dataset for categorization. The results suggest that this method's two-stage strategy can enhance computing time efficiency classification accuracy.

Combining SMOTE with various under sampling algorithms is a typical approach in mixed sampling

schemes. To address the issue of class overlap, Hartono proposes a hybrid sampling method that minimizes overlapping selection, balances multiple classes based on class overlap, and uses minority-based oversampling (M-SMOTE) and editing nearest neighbors (ENN) to sample the minority and majority classes separately. Xu offers a sample-based similarity oversampling and undersampling preprocessing approach, first undersampling the most influential majority class samples and then oversampling the most important minority class samples by examining the safety level created by their nearby regions. It turns out that the proposed algorithm can limit the creation of noisy or overlapping data [29]. Random Balance is a two-class imbalanced data preparation approach that randomly undersamples and SMOTE oversamples data. Janicka proposed the Multi Rand Bal technique based on this, which employs randomly generated priors for sampling instead of class proportions [30]. In his suggested HAR-MI approach, Rodriguez coupled dynamic ensemble selection with Multi Rand Bal, preserving the diversity of data and classifiers while employing a minimal number of classifiers to obtain improved performance. With its tremendous learning capabilities, the classifier-based method combined with oversampling has proved its advantages in handling unbalanced issues [30].

Data Augmentation is effective for preventing models from overfitting, improving model accuracy, and lowering the operational cost of labeling and cleaning the raw dataset. Devaraj & Madian [31] reported new pneumonia medical imaging and infection detection methods. In one of the trials, data augmentation was used. Although data augmentation was promised to improve classification accuracy, most projects lacked data mining techniques. Anand *et al.* [32] correctly described persons and their cardiovascular conditions and took appropriate measures to prevent cardiac absconds. Alternate biological and actual constraints, such as age, gender, cholesterol level, blood pressure, pulse, and location of chest discomfort, can be estimated. The preparation and examination dataset was taken from kaggle.com and includes fourteen separate ascribes. Data is frequently at the center of AI-managed computations.

Devaraj & Madian [31] reported new pneumonia medical imaging and infection detection methods. In one of the trials, data augmentation was used. Although data augmentation was promised to improve classification accuracy, most projects lacked data mining techniques. Aggelides *et al*. [33] presented an interdisciplinary Gesture Recognition case study for recognizing and categorizing motions associated with allergic rhinitis. Allergy diseases, particularly allergic rhinitis, are among the most frequent maladies globally and significantly impede daily activities, including job productivity. Chowdhury *et al.* [34] used data augmentation in an X-ray image dataset that contained 423 COVID-19 samples, 1485 Viral Pneumonia images, and 1579 Normal images. Transfer-learning methodologies were also utilized with the following CNN architectures: MobileNetv2, SqueezeNet, ResNet18, ResNet101, DenseNet201, CheXNet, Inceptionv3, and VGG19 with ImageNet learned weights.

Waheed *et al.* [35] employed an Auxiliary Classifier Generative Adversarial Network (ACGAN) technique to classify COVID-19 X-ray images. The authors fine-tuned the completely connected layer weights and downsized the input images (112 x 112). During the pre-processing step, the author added 403 COVID-19 images and 721 Normal-type images to a dataset. Brunese *et al.* [36] employed VGG16 CNN architecture to identify pneumonia by emphasizing chest radiography areas. Their analysis uncovered 250 COVID-19 photos, 3520 Healthy samples, and 2753 Pneumonia images; the results revealed a sensitivity of 0.960, a specificity of 0.980, an F1-Score of 0.940, and an accuracy of 0.960. Despite the favorable outcome, the authors do not investigate additional options, such as picture pre-processing.

Khan The authors used data augmentation and DarkCovidNet, which was inspired by DarkNet, to diagnose pneumonia in their study [37]. The dataset included 127 COVID-19 Pneumonia pictures, 500 Pneumonia samples, and 500 No-Finding samples. COVID-19 Pneumonia and No-Finding classes attained sensitivity of 0.951, specificity of 0.953, precision of 0.980, F-Score of 0.965, and accuracy of 0.980. When all photos were considered, the findings showed a sensitivity of 0.853, a specificity of 0.921, a precision of 0.899, an F-Score of 0.873, and an accuracy of 0.870.

Rahimzadeh & Attar [38] employed data augmentation to balance the dataset and scaled the pictures (300 300). They used ImageNet transfer learning on the Exception and Resnet50 architectures. The collection includes 180 photographs of COVID-19 Pneumonia, 6.054 images of Pneumonia, and 8.851 images of normal type. The obtained data has an accuracy of 0.914. Despite the small number of COVID-19 Pneumonia pictures, the outcome was representative; nevertheless, cross-validation was not performed in the study.

2.2 Survey on Region of Interest (ROI) and segmentation in Radiology Images

It is vital to train a model using only the most important features, as extraneous features or picture regions degrade the model's performance. As a result, determining the Region of Interest (ROI) is the most important step prior to the training stage. Segmentation comes in handy for this reason because it can separate the irrelevant and superfluous Images or other types of digital signals, such as X-rays, MRI, computer tomography (CT), positron emission tomography, single-photon emission computed tomography, electrical

impedance tomography, and ultrasound, are used to represent a major portion of modern medical data. The collection of massive amounts of such sophisticated image data has resulted in the development of automated medical image processing and analysis.

Medical imaging segmentation is important for obtaining information about the status of various tissues, organs, and other parts of the body [39]. Any lung analysis system's segmentation accuracy and greater decision confidence value for identifying anomalies rely heavily on an effective lung segmentation technique. As a result, the performance of segmentation-based systems is dependent on lung pictures. Medical picture segmentation is difficult due to weak image contrast and artefacts that result in missing or diffuse organ/tissue borders. As a result, this task requires incorporating as much prior information as feasible, such as texture, shape, spatial position of organs, and so on. Manual segmentation is not only time consuming and boring, but it can also be erroneous at times. Expert segmentation has been found to be varied by up to 20% [40]. Therefore, many automatic and semiautomatic techniques have been proposed.

The precision of the segmentation method used to segment the region determines the accuracy in identifying anomalies present in a specific region of medical pictures. As a result, the development of an efficient approach for segmenting numerous regions of medical images is required. The existing approaches for segmenting medical images have limitations because most of them only function on a single type of image. As a result, a strategy for distinguishing several regions of various sorts of medical imaging is more significant. The key advantage of adopting an unsupervised segmentation strategy over a supervised approach is that it is not dependent on labelled training data. This is an essential consideration in medical imaging and related applications [41].

Paper elaborates on the process of segmenting the lung volume within image data using grey level thresholding techniques [42]. The volume criterion is then used in conjunction with multiple grey-level thresholds to identify a collection of three-dimensional module candidates.

The author of the paper proposed a Texture distinctiveness (TD) lesion segmentation technique [43, 44]. It captures textural dissimilarity, distribution by breaking an image into smaller parts, and classification as lesion or skin based on TD map. The lesion region has a high degree of distinction, while the skin region has a low degree of distinction. The authors of paper [45] suggest a Fuzzy Logic-based Bitplane algorithm (FLBP) for extracting lungs from the backdrop of a CT lung picture [45-47]. The collected lungs are then used to identify nodules and undertake additional investigation. Paper [46] proposed a better and automatic approach of extracting skin lesions in a publication. They extracted the ROI region in their technique by integrating pixel and region-based approaches. The authors also used a region-growing strategy to generate results that were related to doctors. In segmenting skin lesions, their system achieves a precision rate of 94.1 percent, a recall rate of 95.3 percent, and a sensitivity rate of 80 percent.

The Paper [48] proposed a unique ultrasonic image segmentation approach based on the curvelet and GLCM features using a spectral clustering algorithm. Gray level co-occurrence matrix-based features and a particle swarm optimization trained feedforward neural network are used. Because the improved GLCM algorithm may improve segmentation accuracy, it has become a frequent way to utilise the optimization algorithm to the optimal segmentation threshold of the multi-threshold algorithm in order to better improve the image segmentation accuracy of the algorithm.

According to the most recent research, imbalanced datasets constitute a key difficulty in the diagnosis of respiratory illnesses using ML approaches. Multi-class imbalance learning on data streams is a relatively unexplored area, with the majority of accessible data stream classification techniques created for the two-class imbalance problem. Some scholars have examined multi-class unbalanced data flow with positive outcomes. However, the problem of uncertainty that may occur in multi-class unbalanced data flow has not been resolved. The amount of data generated in real-world applications is vast, and the complexity is increased. Then there is the issue of notion drift. However, the majority of extant multi-class imbalanced data processing solutions only address one or two of these issues. In this complicated context, more efficient and comprehensive categorization systems must be created. Because early detection of respiratory illness is vital in clinical therapy, locating the Region of Interest (ROI) in radiological images is critical. Real-time radiography images can be low in quality and unclear at times, therefore improving their quality and enhancing their characteristics is crucial in diagnosing respiratory illness at an early stage.

The proposed ML-based technology model will serve as an assisting tool in the medical area by providing solution to image dataset imbalance problem, improvising preprocessing technique to locate ROI and detecting various respiratory ailments using proposed DNN even at the early stages of infection.

3. Proposed Methodology

Researchers developed effective and robust classifiers for distinguishing instances of non-COVID and COVID pneumonia in CT and CXR images using AI-based illness detection approaches. COVID and non-COVID pneumonia Detectors that can categorize and diagnose by drawing bounding boxes on diseased

photos are necessary to construct robust systems. Because of the noisy, inconsistent, and fragmentary data, pre-processing [24] is also required. It is one of the preparatory operations necessary for high step accuracy. Extraneous features or picture areas diminish the model's performance in the case of radiology pictures. As a result, calculating ROI is the most critical step before the training stage. To achieve the goal of pre-processing medical imaging data into improve classification and detection of respiratory illness infection in the human body prior to machine learning algorithms. The suggested system RESDETECT is developed for the identification and analysis of respiratory disease infections in the human body using radiological pictures and is based on machine learning methodologies:

The proposed methodology followed in this research study consists of 5 stages: 1) Radiology Image Data Acquisition, 2) RESP Dataset Construction using data augmentation and proposed image RESP_DATA_BALANCE technique, 3) Image Enhancement and Segmentation using proposed RDD_ROI algorithm 4) Training &feature extraction & classification using proposed custom built 28 layers DNN 5) Validation of the results, with the proposed technique, labelling and respiratory disease detection with real-time time unknown image samples. Figure 1 illustrates these steps.

3.1 Step1: Radiology Image Acquisition

For this study, four medical imaging datasets are taken and a brief detail about these three datasets, namely, CXR images & CT images dataset and RESP dataset are given below.

1) CXR images dataset: CXR (Covid-19 & Pneumonia) collection includes CXR pictures of Covid-19, Pneumonia, & normal patients. Data distribution information for all three classes is shown below in Table 1. The dataset is arranged into two directories (train & test), and each folder has three subfoldeCOVID-19ID19, PNEUMONIA, NORMAL). The dataset comprises 6432 X-ray pictures, with test data being 20 percent of the total images. This dataset is available at https://www.kaggle.com/datasets/prashant268/chest-xray-covid19-pneumonia [49, 50].

2) CT images dataset: Two datasets, namely, the SARS-CoV-2 and the CT-Scan datasets, have been considered. The first data is the CT-Scan dataset, which may be employed to classify and automatically detect COVID-19 on CT scans. COVID-19 Lung CT Scans CT Scan Dataset about COVID-19 and pictures were gathered from COVID19-COVID-19-relateds published on bioRxiv, medRxiv, JAMA, Lancet, NEJM, etc. CTs with COVID-19 abnormalities are chosen by reading the captions of the figure studies. The dataset contains a total of 746 CT scan total images. Shown in Table 2, A CT-Scan dataset is available at: https://www.kaggle.com/datasets/luisblanche/covidct?select=CT_COVID) [51] The SARS-CoV-2 The SARS-CoV-2 data set may be seen at https://www.kaggle.com/datasets/plameneduardo/sarscov2-ctscan-dataset [52]

3) RESP Dataset (X-ray images): The complete dataset consisted of labeled 316 chest X-ray images with 102 normal images, 110 bacterial pneumonia images, and 104 viral images of COVID-19 in shown in Table 3 and 60 unlabeled images 20 from each label class are used for the proposed system validation purposes. The entire dataset was acquired from a local hospital that contained chest X-ray images of various conditions. The dataset was quite imbalanced and limited.

Figure 1. RESDETECT System Flow Diagram

Table 1. Data Information of Chest X-Ray

Data	Covid19	Pneumonia	Normal	Total
Training	460	3418	1266	5144
Testing	116	855	317	1288

Table 2. CT image data information

Dataset Name	Covid images	Non-covid images	Total images
COVID-CT dataset	349	397	746
SARS-COV-2	1252	1229	2481

Table 3. RESP Dataset image data information

Dataset Name	Pneumonia Infected Image Samples	COVID Infected Image Samples	Normal Image Samples	Total images
Training	88	83	81	252
Testing	22	21	21	64

3.2 RESP Dataset construction majorly focuses on 2 steps:

a) Image Data augmentation

b) Image Data Balancing

3.2.1 Image Data augmentation

One of the most significant difficulties encountered in the chest radiology image classification problem is the scarcity of images, making the datasets unbalanced. We adopted data augmentation to overcome this problem, which encompasses techniques that improve the size and quality of training datasets. In this way, deep learning models can improve learning by enhancing generalization.

Data Augmentation is useful to prevent models from overfitting, if the initial training set is too small, to improve the model accuracy, and to Reduce the operational cost of labelling and cleaning the raw dataset during the literature survey, different data augmentation techniques were studied. By understanding, features and usability proposed system uses four types of data augmentation methods to overcome unbalanced datasets.

3.2.1.1 Rotation

Rotation considers transformation matrix R_T

$$R_T = M * [x\ y\ 1]_T \quad (1)$$

The transformation matrix is a 2 x 3 matrix, which is multiplied by [x y 1] where (x,y) are coordinates of the point. The idea of having a 1 is to facilitate shearing, multiplying a 2 x 3 matrix with a 3 x 1 matrix leaves us with a 2 x 1 matrix containing the new point coordinates. The transformation matrix can be also used to get the coordinates of a point after rotation about the center of the image. The transformation matrix for rotating a point by angle looks like. This the point situated at the coordinates (x, y) in the new image is equal to the point (xp, yp) in the input image:

$$\mathrm{xp} = \mathrm{x} * \cos(\mathrm{angle}) - \mathrm{y} * \sin(\mathrm{angle}) \quad (2)$$

$$yp = \mathrm{x} * sin(angle) + \mathrm{y} * cos(angle \quad (3)$$

This can be used to do a rotation; however, the center of the rotation will be at coordinate (0, 0). To change the coordinates of the center of the rotation, we need to shift the coordinates before the rotation and after the rotation:

$$xp = (x - center\_x) * cos(angle) - (y - center\_y) * sin(angle) + center\_x \quad (4)$$

$$yp = (x - center\_x) * sin(angle) + \left(y - center_y\right)^* cos(angle) + center_y \quad (5)$$

3.2.1.2 Flipping the images horizontally

A flip (mirror effect) is done by reversing the pixels horizontally or vertically. For the horizontal flip, the pixel situated at coordinate (x, y) will be situated at coordinate.

$$New\ Image(x, y) = (width - x - 1, y) \quad (6)$$

3.2.1.3 Translation

It considers the translation matrix (translation matrix) using a 2x3 NumPy array. The first row represents the x-shift (horizontal shift), and the second row represents the y-shift (vertical shift)

3.2.1.4 Image Edge detection

Edge detection is a very important task for healthcare industries, deep learning image classification projects, and Object detection projects. During the literature review, different edge detection techniques like Histogram equalization, Gaussian blurring, Bilateral filter, and Adaptive masking are studied, and the experiment is carried out with different techniques to check the performance of the proposed system and it has been observed the that RESDETECT system performs well with Gaussian blurring edge detection

technique which can be presented in below mentioned Table 7.

Figure 2 shows radiology image dataset before data augmentation and Figure 3 displays images after application of data augmentation techniques like rotation, flipping, translation & Gaussian Blurring image edge detection technique to generate augmented images.

3.2.2 Image Data Balancing

In medical imaging datasets, most often the data is collected from various sources, and not all diseases are as prevalent as others, so the datasets are imbalanced often. During the literature survey, we studied different image dataset balancing techniques like Weight loss, under sampling and, sampling etc. Since number of images in data, the set is less in numbers so we experimented proposed model with on oversampling image data balancing technique the proposed method imported vises traditional image data oversampling technique by generating artificially augmented images. To an implement oversampling data balancing the technique in Respiratory Disease Detection algorithm RESP_DATABALANCE is proposed.

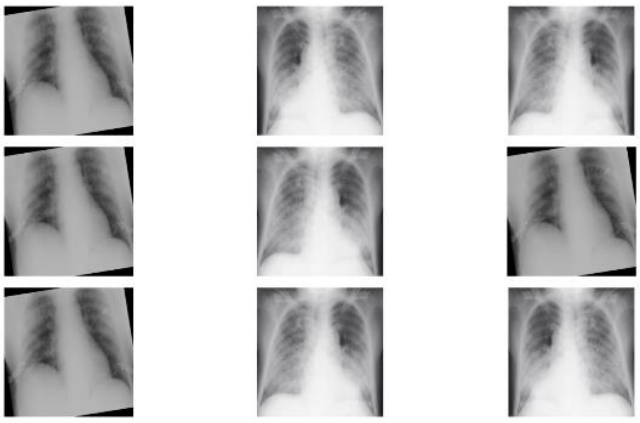

Figure 2. Radiology Image Dataset before data augmentation

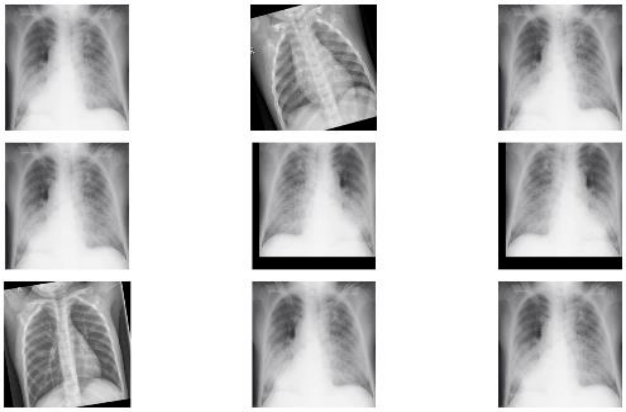

Figure 3. Radiology Image Dataset after data augmentation

Algorithm: RESP_DATA_BALANCE
Input: Imbalanced Radiology Image Dataset
Steps: 1. Load imbalance image dataset 2. Initialize 1-D character string array S of each image label as S={l1, l2,l3,….ln} 3. Calculate the length of the S to acquire the count of image labels in the input image dataset as Label_Count =Length(S) 4. Initialize integer count array as Count [Label count] a. Repeat i=0 < Label_Count b. Count number of images for label S[i] as Count [i]=sum (images in S [i])

- ❖ Repeat Step 4 for all the image label dataset

5. Evaluate the Majority label class as Major label class M =Lable S[i] where (Count[i]) is maximum and Number of majority class images Mi= Max (Count[i])
6. Calculate the difference for each minor laclasssses as
   - a Initialize difference array Diff [label count]
   - b Initialize j=0 to label_count
   - c Diff[i]=Count[i]-Mi
   - ❖ Repeat step 6a,6b,6c for each label class
7. Repeat k=0 to Label_count
   - a. If Diff[k]>0

   Randomly select the image of label class S[k]
   - b. Apply data augmentation to the image as
     - I. Rotation
     - II. Flipping the images horizontally,
     - III. Translation, with random settings both for the x and y-axis,
     - IV. Edge detection using Gaussian Blurring technique
   - c. Append image in label class S[k]
   - d. Count[k]=count[k]+1
   - e. Diff[k]=count[k]-M

- ❖ Repeat step 7 for each minor label class image dataset until each label class reaches diff 0

Output: Balanced Radiology Image Dataset

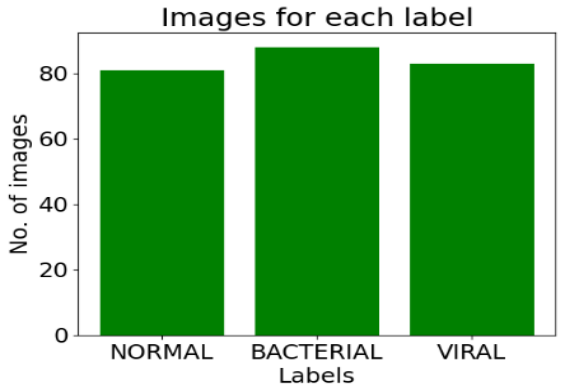

Figure 4. Unbalanced Radiology Image Dataset

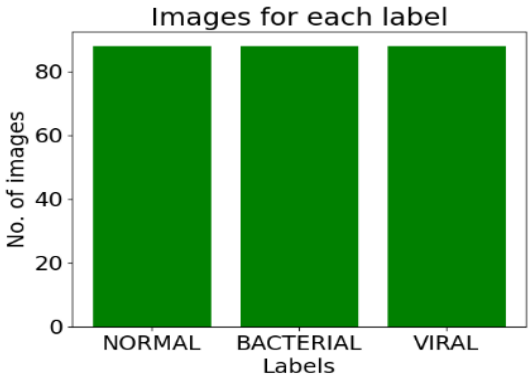

Figure 3. Balanced Radiology Image Dataset on application of RESP_DATA_BALANCE

In the proposed method, oversampling should be done on trainingning data, and not on test data as if test data contains artificially generated images, the classifier results we will see would not be a proper interpretation of how much the network learned. So, the better method is to first split the train and test data and then oversample only the training data.

As displayed in Figure 4, the training set has 81 normal images, 88 bacterial pneumonia images, and 83 viral pneumonia images. So finally, we have a balance in the training dataset. We have 88 images in all three classes displayed in Figure 5. So, we have solved the Class Imbalance Problem with this step.

3.3 Image Enhancement and Segmentation using the proposed RDD_ROI algorithm

Image enhancement increases the raw data's quality and informational content before processing. Several levels of compression were utilized to store digitized pictures in this method. GLCM is an excellent discriminator when comparing various images, although this cannot be said for image quality. Ultrasound pictures often exhibit many granular features like texture, and the study of ultrasound images is akin to the challenge of texture analysis. However, the image's textural properties include qualities like smoothness, fitness, & coarseness of a particular pattern. There are several texture feature analyses approaches available. Earlier results show GLCM performs better in image feature extraction.

3.3.1 GLCM (Gray-Level Co-occurrence Matrix)

It is a typical technique for defining texture by analysing spatial correlation properties of grayscale. Due to the repetitive occurrence of grey distribution in spatial position, there would be a special gray connection among 2 pixels at a given distance, i.e., spatial correlation features of grey in the image. A grayscale histogram is a statistical outcome of a single pixel on the image having a given grayscale; however, GLCM is formed by statistically establishing a state in which 2 pixels divided by a specified distance on the image each have a particular grayscale [28].

Take each point (x, y) in the picture (N × N) as well as the point that deviates from it (x + a, y + b) & set the gray value of the point pair to (g1, g2). When a point (x, y) is moved throughout the image, many (g1, g2) values are acquired. K-square describes the sequence of grayscale values and the combination (g1, g2). Count no. of occurrences of each (g1, g2) value & assemble them in a square matrix; next, normalize total no. of (g1, g2) to occurrence probability P (g1, g2); this is referred to as GLCM. Under certain conditions, distance difference values (a, b) may be combined with other variables to produce a joint probability matrix. The texture's periodic distribution defines values (a, b). Finer textures use small difference values like (1, 0), (1, 1), as well as (2, 0); when a = 1 and b = 0, a pixel pair is horizontal, which corresponds to 0° scanning. When a = 0 and b = 1, a pixel pair is vertical, known as 90° scanning. When a = 1 and b = 1, the pixel pair is right diagonal, sometimes referred to as 45-degree scanning. The left diagonal pixel pair corresponds to 135° of scanning when a = -1 and b = 1. This approach transforms (x, y) spatial coordinates to the description of a "gray pair" (g1, g2) based on the likelihood of simultaneous occurrence of two gray levels per pixel, producing GLCM.

The following is an approach for normalizing GLCM

$$(g1, g2) = \frac{p(g1,g2)}{R} \tag{7}$$

The calculation process of

$$RR = \begin{cases} N(N-1) & \theta = 0 or \theta = 90 \\ (N-1)^2 & \theta = 45 or \theta = 135 \end{cases} \tag{8}$$

If the picture consists of blocks of pixels with comparable gray values, the diagonal elements of GLCM would have relatively large values; if grey values of image pixels vary locally, the elements that deviate from the diagonal can have larger values.

In the case of respiratory disease diagnosis using radiology images. To locate Region of Interest (ROI) is important, (Respiratory Disease Detection Region of Interest) RDD_ROI algorithm is proposed in image enhancement and segmentation relies on a statistical correlation between neighbouring pixels. Linear dependency is the most basic type of dependency, and the proposed method considers linear dependency of neighbouring pixels of a given kernel window size. Features extracted for important pixels are then given to all pixels in their surrounding a weight matrix hence it reduces overall computation time during the image feature extraction. The feature vector related to every non-key pixel is a weighted sum of feature vectors for all weighting kernel windows containing that pixel. To speed up the calculation and decrease the amount of time spent on it, we compute Gray-level co-occurrence matrix (GLCM) features for essential pixels also then utilize interpolation to estimate GLCM features for other pixels.

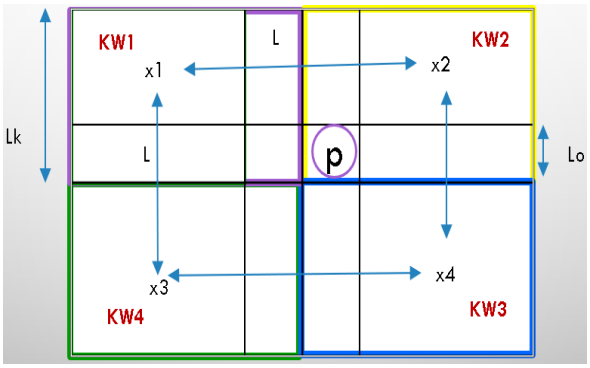

Figure 6. Four Lk×Lk weighting kernel windows

Figure 6. displayed four Lk×Lk weighting kernel windows (Kwi) with the overlap of length Lo. Here, features of pixel p are the weighted sum of that of xi.

$$f(p)\sum_{l=1}^{n} ai(p)f(xi) \quad (9)$$

where,

f(p)= feature vector of non-key pixel p

xi = is the key pixel located at the center of each of the overlapping weighting windows which include p;

ai(p) = weight associated with pixel p in the weighting window centered at xi

Before being sent to the classifiers, features are normalized such that they fall within the range 0–1, and the classifiers all get the identical set of features. In this work, the GLCM method extracts seven texture features like homogeneity, correlation, dissimilarity, contrast, entropy, energy, and ASM of the radiology images.

3.4 Unsupervised segmentation and clustering of radiology images

Image Segmentation (IS) is a technique of splitting the digital image into discrete sections containing pixels (also called superpixels) with appropriate attributes. Numerous studies have been conducted in the field of IS using clustering. During the literature survey, multiple image segmentation techniques like K-Means Clustering, Adaptive Thresholding, Watershed, and Canny Edge Detection were studied. Our research study proposes Respiratory Disease Detection Region of Interest (RDD_ROI) image segmentation technique, which considers pixel correlations followed by K-means clustering for the image segmentation locate Region of Interest (ROI). The pixels with similar properties are clustered together in image segmentation. RDD_ROI performs better with RESDETECT system compared to other image segmentation techniques.

3.4.1 K-means clustering

The clustering of a picture is the most effective image segmentation method. After extracting features, they are grouped into well-separated clusters depending on each image class. The objective of the clustering method is to generate partitioning decisions depending upon an initial set of clusters that is updated after every iteration. K-means is an effective approach for clustering. Based on initial cluster centroids, it is utilized to split related data into groups. This algorithm first selects k data values as initial cluster centres, then calculates the distance among every cluster centre & every data value and assigns it to the nearest cluster, updates the average of each cluster, and repeats until the condition is no longer satisfied. K-means clustering aims to split data into k clusters where every data value belongs to the cluster with the closest mean [30]. The algorithm for k-means (in algorithm1), where every cluster's center is denoted by the mean value of objects in a cluster [31].

Algorithm: K-Means Algorithm
Input: k: No. of clusters. D: Dataset containing n objects. **Output:** A set of k clusters.
Method: Step1. Select at random k objects from D to serve as first cluster centers. Step 2. Repeat Step 3. Re (assign) every object to the cluster to which it is most closely related depends upon the mean value of objects in the cluster, using the following formula. Step 4. Determine the average value of every cluster's objects and update cluster means. Step 5. Until no change $the\ J = \sum_{n=1}^{j}\sum_{m=1}^{i}\left\|X_m^{(n)} - C_n\right\|^2$ (here, $\left\|X_m^{(n)} - C_n\right\|^2$ is a calculated distance (intra) between data point X_m m as well as the cluster center C_n, it indicates the distance between the cluster center and their n data points. Intra-term is employed to quantify the density of clusters. Inter-term represents a minimal distance between cluster centroids.

Algorithm: Respiratory Disease Detection Region of Interest (RDD_ROI)
Input: Radiology images datasets (X-ray images & CT images)
Output: Enhanced and segmented radiology Images

Steps:

1. Input radiology image datasets
2. Transform the input image into a grayscale image
3. Requantize Grayscale Image
4. Image resizing into 256X256
5. Characterize the texture of picture using the GLCM method
6. Generate Feature Matrices for the key pixel value of specified Kernel Windows size
7. Extract features like Correlation, Contrast, Homogeneity, Energy, Variance, and entropy, are features extracted from GLCM matrices Repeat steps 3 to 5 for the remaining neighboring key pixels at a distance of L
8. Calculate the weight associated with non-key pixels
9. Select no. of clusters that correspond to k. For the proposed algorithm, K=2 is considered.
   a. Cluster 1=Foreground Bright Area
   b. Cluster 2= Background Dark Area
10. Allocate data points at random to any of the k clusters.
11. Next, compute the clusters' centers.
12. Compute the distance between every data point and the cluster's center.
13. Based on the distance between every data point and cluster, reassign data points to clusters closest to them.
14. Calculate the new center of the cluster once again.
    - ❖ Repeat steps 10, 11, & 12 until data points no longer alter clusters or until the allotted number of iterations has been reached.

Output: Enhanced and segmented radiology images.

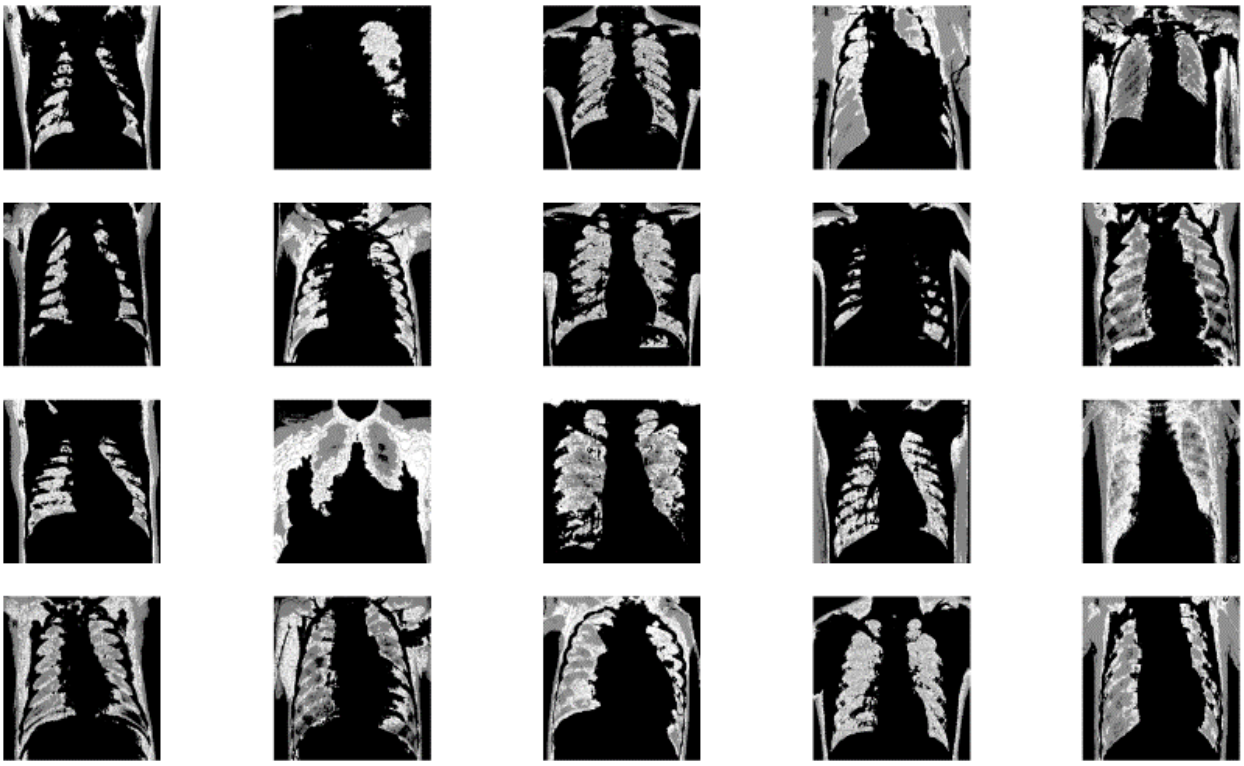

Figure 7. Enhanced and segmented radiology images after the RDD_ROI algorithm

Layer	Filters	Kernal size	Padding	Output shape	Activation function
Input	-	-	-	256 x 256 x 1	-
Conv 1	32	3 x 3	Same	256 x 256 x 32	ReLu
BatchNormalization	-	-	-	256 x 256 x 32	-
MaxPooling	-	3 x 3	-	85 x 85 x 32	
Dropout	rate = 0.25	-	-	85 x 85 x 32	-
Conv 2	64	3 X 3	Same	85 x 85 x 64	ReLu
BatchNormalization	-	-	-	85 x 85 x 64	
Conv 3	64	3 X 3	Same	85 x 85 x 64	ReLu
BatchNormalization	-	-	-	85 x 85 x 64	-
MaxPooling	-	2 x 2	-	42 x 42 x 64	-
Dropout	rate = 0.25	-	-	42 x 42 x 64	-
Conv 4	128	3 x 3	Same	42 x 42 x 128	ReLu
BatchNormalization	-	-	-	42 x 42 x 128	-
Conv 5	128	3 x 3	Same	42 x 42 x 128	ReLu
BatchNormalization	-	-	-	42 x 42 x 128	-
MaxPooling	-	2 x 2	-	21 x 21 x 128	-
Dropout	rate = 0.25	-	-	21 x 21 x 128	-
Flatten	-	-	-	56448	
Dense	-	-	-	1024	ReLu
BatchNormalization	-	-	-	1024	
Dropout	rate = 0.25	-	-	1024	
Dense	-	-	-	No of classes	Sigmoid

Figure 8. RDD_DNN model architecture details

Therefore, enhanced and segmented images displayed in Figure 7 shows that, RDD_ROI improvises existing GLCM followed by K-means Clustering for image enhancement and segmentation to prepare any respiratory diseases radiology images ready for training testing and validation, using Deep Neural Network (DNN).

3.5 Feature Extraction & Classification using Respiratory Disease Detection_DeepNeural Netwok (RDD_DNN)

The proposed Deep Neural Network model, RDD_DNN custom-built DCNN model designed by understanding importance of DNN layers and setting parameters to achieve efficient performance of model.

RDD_DNN is suitable for image classification tasks with multiple classes. The architecture includes multiple convolutional layers with pooling and dropout, followed by fully connected layers and an output layer with a sigmoid activation function. The model uses Batch Normalization to stabilize training and improve generalization. Figure 8 displays the proposed RDD_DNN model by setting the parameters. Different layers are used in this architecture, and their description is discussed below.

3.5.1 Different Layers in DCNN

3.5.1.1 Convolution Layer

- The term "convolutional layer" suggests that the network performs convolution, a mathematical technique.

3.5.1.2 Max Pooling Layer

- The pooling layer controls overfitting by slowly decreasing the spatial dimension of representation, no. of parameters, memory footprint, and amount of processing in the network.
- Pooling is a crucial part of CNNs for object identification.

3.5.1.3 Batch Normalization

- The batch normalization procedure restricts the layer's output to a defined range, imposing zero mean & one standard deviation.
- This acts as regularization, enhancing the neural network's stability and expediting the training process.

3.5.1.4 ReLu Layer

- ReLU is an acronym for Rectified Linear Unit that uses non-saturating activation function f(x)=max (0, x).
- It imparts nonlinearities to decision function & network without influencing the receptive fields of convolution layers.
- ReLU is frequently favoured over other functions since it trains neural networks multiple times quicker while maintaining generalization accuracy.

3.5.1.5 Loss Layer

- "Loss layer" or "loss function" explains how training penalizes the difference between the network's projected output and actual data labels.
- Based on an individual task, different loss functions may be used.

3.5.1.6. Dropout Layer

- A dropout layer is a regularisation layer initially described in [32].
- It may be implemented on any network layer.
- The primary goal of regularisation is to reduce to zero weights that do not contribute to the accuracy of the model.

3.5.1.7 Fully Connected (FL) Layer/Dense Layer

- Finally, FC layers are utilized to make categorizations.
- The primary goal of this layer is to categorize the original picture based on all the information retrieved from the preceding layers.
- A SoftMax or sigmoid function is used to output target probability after a network.

3.6 Working Principle

The working principle of the RDD_DNN model for layer-wise operation is outlined as follows:

- First input image of size 256 x 256 is fed to the Input Layer.
- Convolutional layer Conv1 uses 32 filters to generate the features map.
- The model starts with a 2D convolutional layer with 32 filters of size (3, 3), using the ReLU activation function. It employs zero-padding ('same') to keep the spatial dimensions unchanged after the convolution and Batch Normalization to normalize the activations.
- MaxPooling2D layer with pool size (3, 3) is applied to reduce the spatial dimensions and control overfitting through the Dropout layer with a dropout rate of 0.25.
- The model continues with two more sets of Convolutional, Activation, Batch Normalization, MaxPooling, and Dropout layers. The second set has 64 filters, and the third set has 128 filters.
- After these convolutional layers, the model adds a flattened layer to convert the 3D output into a 1D vector.
- A fully connected layer (Dense) with 1024 units and ReLU activation is added. Batch Normalization and Dropout (dropout rate of 0.5) are applied after this layer to further regularize the model.
- The output layer consists of a Dense layer with several neurons equal to the number of classes in the classification problem. It uses the sigmoid activation function to produce probabilities for each class independently.

Deep Learning features of the model helps in the identification of the early stage of respiratory diseases and helps radiology person to label unknown sample and diagnose the disease.

3.7 Labelling/ Respiratory Disease Prediction

The final step of RESPDETECT system considers classification/prediction of unknown radiology image samples for the presence or absence of respiratory disease in human body.

Figure 9 (a) are unknown radiology image samples from Validation dataset and Figure 9(b) displays prediction of class label for each unknown sample. In this way proposed RDD_DNN model able to label unknown samples and detect the presence or absence of respiratory diseases like COVID, Pneumonia etc.

4. Results and Analysis

The experiments have been done using Python programming. These experiments have been done on CXR images & CT scan images and RESPDATASET x-ray images and analysed results for Covid-19 classification. The section displayed the results of segmented images and classified results of different collected image data.

4.1 Experimental Setup

The experiments have been run on the Jupyter Notebook environment. It is an initial step to gather radiology images. In the initial step of the process, a set of X-ray & CT images (infected & non-infected) are extracted from the public database at [50-52]. The picture obtained is in its raw format. An abundance of noise is detected in the acquired picture. It must be pre-processed to enhance contrast transparency and background noise separation. The dataset is partitioned into 3 parts with 60% training, 20% validation & 20% test set. For the classification model, some hyperparameters like binary cross entropy as loss function, Adam optimizer, 32 batch size & 100 epochs are tuned for the image dataset. This is the process of making predictions using the trained model on unlabelled data. We then measure the accuracy with which the model made these predictions for classification tasks.

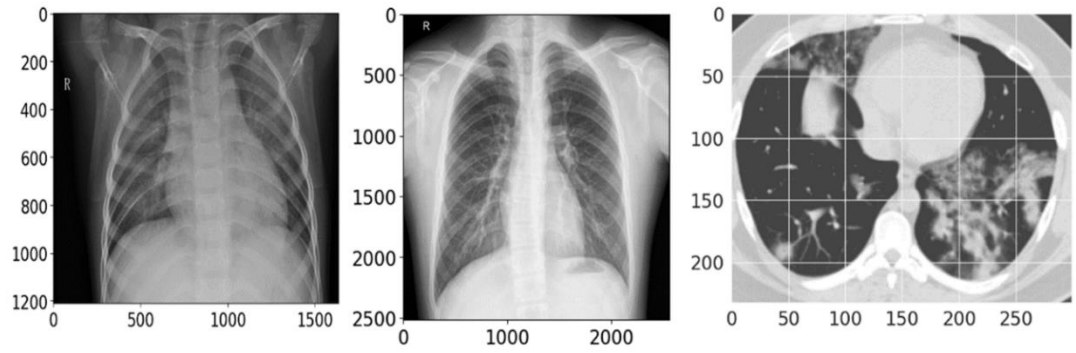

(a) Sample Input Unlabelled Radiology Images

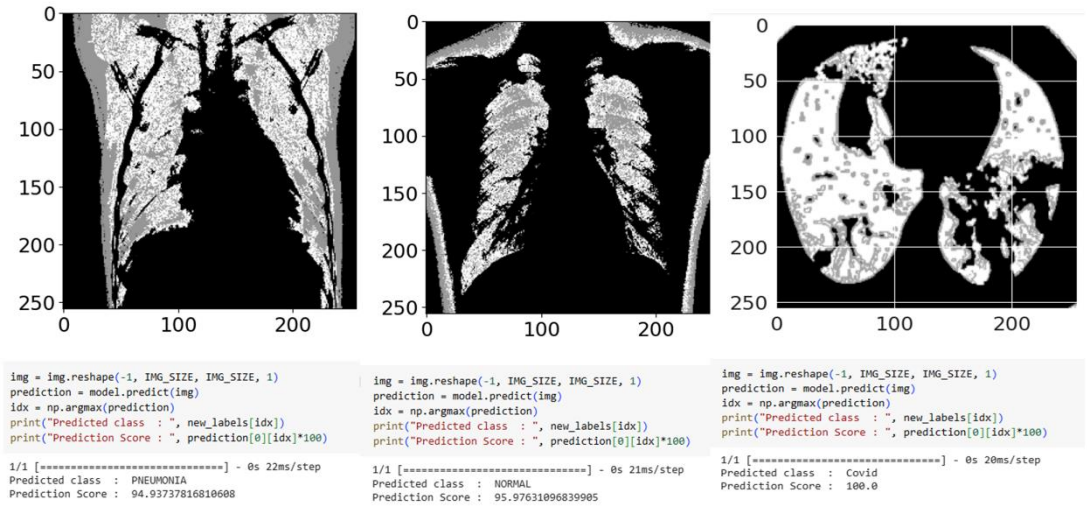

(b) Output Labelled Radiology Images

Figure 9. Respiratory Disease prediction with RDD_DNN model

4.2 Performance Metrics

The classification performance report evaluates the quality of a proposed classification model. It works both for binary and multi-class classification of COVID-19 detection. This report is generated for RDD_DNN model or as a comparison.

4.2.1 Accuracy

Accuracy is a metric that may be used to evaluate classification methods. Informally, accuracy is the proportion of correct predictions made by our model. It is a correlation between the accuracy of value and information

$$\boldsymbol{Accuracy} = \frac{(\mathrm{TP} + \mathrm{TN})}{(\mathrm{TP} + \mathrm{TN} + \mathrm{FP} + \mathrm{FN})} \quad (11)$$

Where, TP = True Positive, TN = True Negative, FP = False Positive, & FN = False Negative.

4.2.2 Precision

It measures the proportion of positively categorized occurrences or samples that were accurately classified. Therefore, the precision calculation formula is as follows:

$$\boldsymbol{Precision} = \frac{\mathrm{TP}}{(\mathrm{TP} + \mathrm{FP})} \quad (12)$$

4.2.3. Recall

It is a measure utilized to assess the prediction performance of the classification model on a certain class of interest, commonly named positive.

$$\boldsymbol{Recall} = \frac{\boldsymbol{TP}}{(\boldsymbol{TP} + \boldsymbol{FN})} \quad (13)$$

4.2.4 F1-Score

It represents the harmonic mean of precision & recall. It integrates recall & precision into a single number. We calculate an average of recall and precision for the F1 score.

$$\boldsymbol{F1 - Score} = 2 * \frac{\boldsymbol{Precision} * \boldsymbol{Recall}}{(\boldsymbol{Precision} + \boldsymbol{Recall})} \quad (14)$$

4.2.5. Area Under the Curve (AUC)

AUC is an acronym for "Area under the ROC Curve." Thus, AUC evaluates the full 2D area under the complete ROC curve (consider integral calculus) from (0,0) to (1,1). (1,1). AUC is a metric that assesses the capacity of the classifier to differentiate between different types of data. The larger the AUC, the greater the model's capacity to distinguish between positive and negative classifications. The receiver Operating Characteristic (ROC) curve shows the performance of the classification model across all classification levels. The graph illustrates two factors:

- True Positive Rate (TPR)
- False Positive Rate (FPR)

TPR is a synonym for recall; hence it is described by this formula, which is given below:

$$\boldsymbol{TPR} = \frac{\mathrm{TP}}{(\mathrm{TP} + \mathrm{FN})} \quad (15)$$

The formula for FPR is described below

$$\boldsymbol{FPR} = \frac{\mathrm{FP}}{(\mathrm{FP} + \mathrm{TN})} \quad (16)$$

A ROC curve compares TPR to FPR at various classification levels.

4.3 Results and Comparison

In the analysis of the results, conventional CT scans & CXR pictures were compared with those of COVID-19-affected individuals. This section discusses the preprocessing and classification results after applying the proposed techniques to radiology scan images from datasets. Performance is observed with the RDD_DNN model based on the accuracy and loss curve and other classification results.

4.3.1. Experimental Analysis of RDD_DNN with diffèrent datasets

Experimental evaluation presented in Table 4 and Table 5 presents performance analysis of RDD_DNN with Datasets mentioned above. It acheives 99.12% and 99.94% training accuracy with CT images and Xray images also 99% with RESP Dataset and 95.17%, 93.97% and 93.75% as Validation accuracy respectively

Table 4. Analysis of RDD_DNN performance with all the dataset

Dataset	Training accuracy	Training Loss	Validation Accuracy	Validation Loss
CT images	0.9912	0.0204	0.9517	0.3719
Xray images	0.9994	0.0081	0.9397	0.6045
RESP Dataset (X-ray images)	0.9900	0.0390	0.9375	0.2341

Table 5. Classification performance results of RDD_DNN with radiology datasets

Dataset	Precision	Recall	F1-Score
CT-images	0.95	0.93	0.94
Xray images	0.94	0.91	0.93
RESP Dataset(X-ray images)	0.8914	0.8817	0.8823

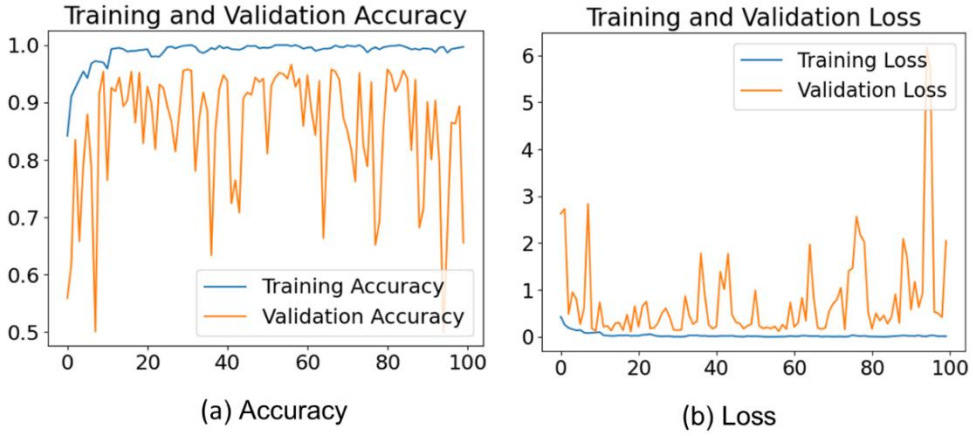

Figure 10. Training & validation accuracy & loss of proposed RDD_DNN model on CT images

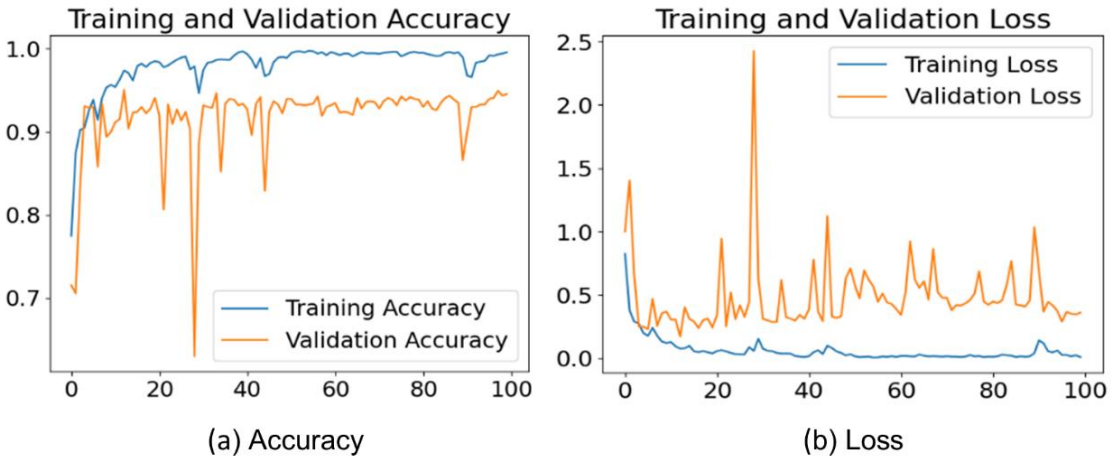

Figure 11. Training & validation accuracy & loss of proposed RDD_DNN model on X-ray images

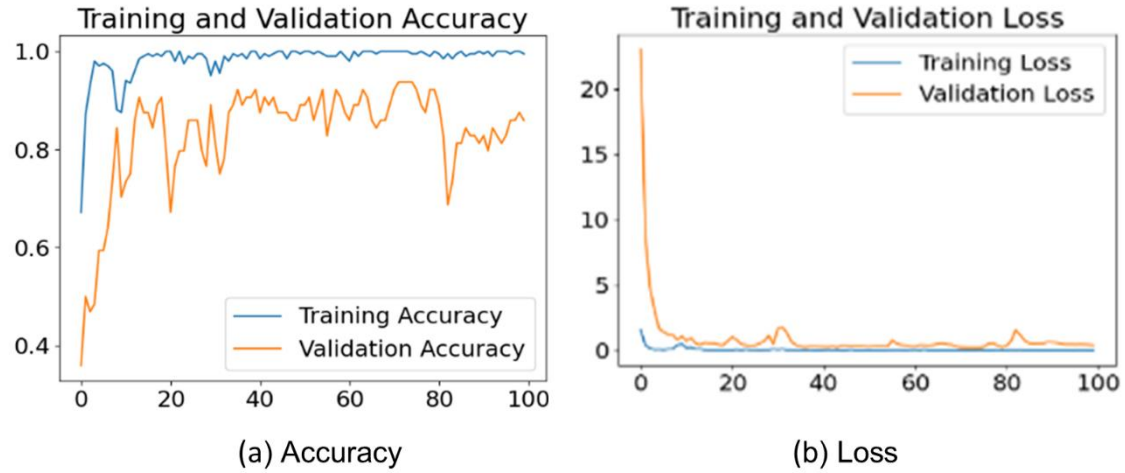

Figure 12. Training & validation accuracy & loss of proposed RDD_DNN model on RESP Dataset

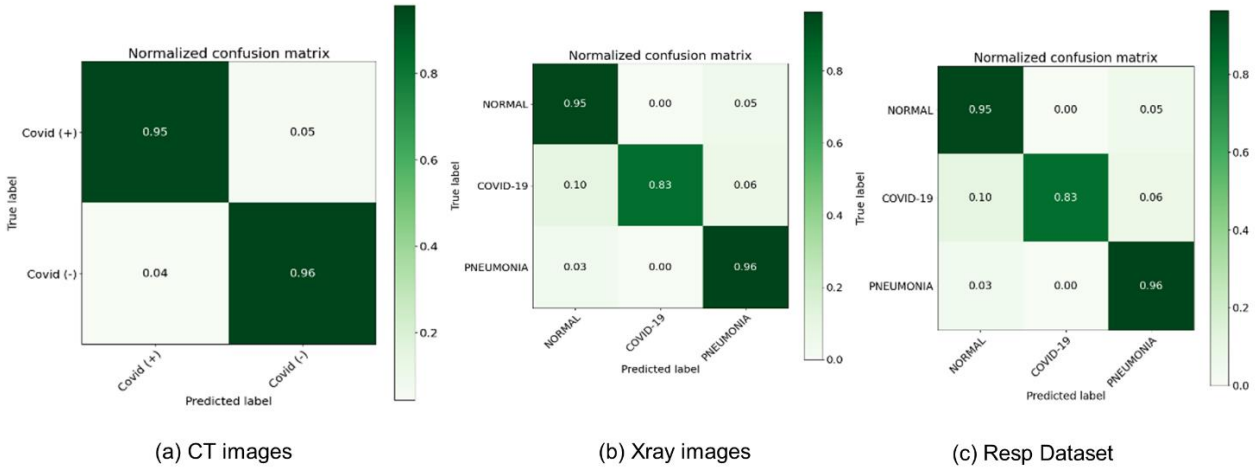

Figure 13. Confusion matrix of RDD_DNN model on radiology image datasets

Table 6. Experimental Analysis of RDD_DNN with Different Image Enchantement and Segmentation Techniques

Technique	Accuracy	Precision	Recall	F1-Score
K-Means Clustering	0.9513	0.9214	0.9324	0.9327
Adaptive Thresholding	0.9314	0.9613	0.9018	0.9322
Watershed	0.8911	0.8613	0.8724	0.8722
Canny edge Detection	0.8841	0.8413	0.8514	0.8459
Proposed RDD_ROI	0.9658	0.9414	0.9612	0.9523

Table 7. Experimental Analysis of RDD_DNN with Different Image Edge detection techniques

Image Edge Detection Technique	Accuracy	Precision	Recall	F1-Score
Without Augmentation	91.32	0.8713	0.8621	0.8623
Gaussian Blurring	94.43	0.8924	0.8813	0.8814
Histogram Equalization	93.14	0.8834	0.8711	0.8712
Bilateral Filter	90.12	0.8613	0.8453	0.8451
Gaussian Blurring	94.43	0.8924	0.8813	0.8814

Table 8. Experimental Analysis of RDD_DNN with RESP_DATA_BALANCE Algorithmes with different radiology datasets

Technique	Dataset	Accuracy	Precision	Recall	F1-Score
Without Data Balancing and Data Augmentation	CT-images	96.58	94.15	95.56	94.74
	X-ray images	95.13	95.21	94.57	94.76
With Traditional Data Balancing and Data Augmentation	CT-images	96.62	94.13	95.74	94.85
	X-ray images	95.29	95.22	94.65	94.89
With RESP_DATA_BALNCE	CT-images	97.63	96.12	96.76	96.35
	X-ray images	96.89	96.21	96.64	96.69

Table 9. Comparative analysis of the proposed model with other techniques for CT-scan images

Model	Training loss	Training accuracy	Validation loss	Validation accuracy
EfficientNetB0	0.2919	0.9022	0.3985	0.8330
EfficientNetB3	0.2614	0.9103	0.2343	0.9155
Proposed RDD_DNN	0.0204	0.9912	0.3719	0.9517

Table 10. Classification performance results in comparison for CT-scan images

Model	Precision	Recall	F1-Score	AUC
EfficientNetB0	86.61	87.30	86.96	86.71
EfficientNetB3	93.16	92.80	92.98	92.54
Proposed RDD_DNN	0.95	0.93	0.94	0.94

Table 11. Comparative analysis of the proposed model with other techniques for X-ray images

Model	Training Acc	Training Loss	Val. Acc	Val. Loss
InceptionV3	0.9051	0.2288	0.9092	0.2397
ResNet	0.8989	0.2338	0.8820	0.3102
Xception	0.9349	0.1752	0.9293	0.1979
Proposed RDD_DNN	0.9994	0.0081	0.9397	0.6045

Table 12. Classification performance results in comparison of X-ray images

Model	Precision	Recall	F1-Score
Inception V3	0.91	0.90	0.90
ResNet	0.92	0.92	0.91
Xception	0.93	0.92	0.92
Proposed RDD_DNN	0.94	0.91	0.93

Figure. 10,11 &12 depict training & validation loss & accuracy analyses of the RDD_DNN model applied to our selected datasets. Fig. 10 (a),11(a) and 12(a) depict model accuracy for the RDD_DNN model as it increases with successive epochs; training accuracy is greater than validation accuracy. Figures 10(b),11(b) and 12(b) depict validation loss for the RDD_DNN model as it decreases with successive epochs, whereas training loss was continuously reduced from 0-100 iterations. Training & validation loss curve results for the proposed model are 0.0204 and 0.5954for CT images; the comparison results found that the proposed model has achieved 95% precision, 93% recall, 94% F1-score, and 0.94 AUC on CT images

Figure. 13(a) shows the normalized binary confusion matrix on the CT scan test set using the RDD_DNN model to predictCOVID (+) or COVID (-). This matrix plotted between a true label and a predicted label for these two classes of COVID from 0.0 to 1.0 scale. The matrix shows a true positive value of 0.95 for the COVID (+) class and a true negative value of 0.93 for the COVID (-) class. Figure. 13(b) demonstrates the normalized confusion matrix of a testing set of the RDD_DNN model to multiclassification on the x-ray images dataset. This matrix plotted among normal, COVID-19, and Pneumonia classes from 0.0 to 1.0. The matrix shows the highest true positive value for the normal class getting 0.85, for the COVID class getting 0.91, and 0.98 for the pneumonia class. Also, Fig. 13(c) demonstrates the normalized confusion matrix of a testing set of the RDD_DNN model to multiclassification on the x-ray images dataset. This matrix plotted among normal, Viral Pneumonia (COVID-19), and Bacterial Pneumonia classes from 0.0 to 1.0. The matrix shows the highest true positive value for the normal class getting 0.89, for the Viral Pneumonia (COVID-19), class getting 0.93, and 0.84 for the Bacterial pneumonia class.

Table 6 presents the experimental evaluation of RDD_DNN with different image enhancement and segmentation techniques and the results show that our proposed RDD_ROI algorithm gives better results with 96.58% accuracy,0.9414 precision, 0.9612 recall, and 0.9523 F1-Score.

Table 7 presents an experimental evaluation of RDD_DNN with different image edge techniques and results show that Gaussian Blurring gives better results with 94.43% accuracy,0.8924 precision, 0.8813 recall, and 0.8814 F1-Score.

Table 8 presents an experimental evaluation of RDD_DNN without data augmentation, traditional data augmentation where overfitting is achieved by copy method to balance dataset and proposed RESP_DATA_BALNCE algorithm and results show that accuracy and performance parameters got improved with our RESP_DATA_BALANCE algorithm.

In Table 9, we provide the outcomes of the proposed model using models presented in Reference [53, 54]. On both datasets, including SARS-Cov-2 and CT-Covid, it is possible to notice that EfficientNet-B0 has worse performance when compared to EfficientNet-B3, which is discussed in the literature. We present a deeper network to avoid overfitting while training existing models. When a deeper network (see "Proposed RDD DNN" in Table 4) is used as opposed to existing models, an improvement in all reported figures is noticed. The best model utilizes the Proposed RDD_DNN input size of 256x256. However, EfficientNet-B3 provides good training and validation accuracy with loss results but has not performed better than the proposed **RDD_DNN** model.

The best-suggested model is compared to other models shown in Table 10. Despite the accuracy results presented for EfficientNetB0 and EfficientNetB3 with the

proposed model in table 4 on both datasets of CT scan, both evaluated their models with additional performance parameters to classify the performance of covid detection (COVID (+) and Covid (-)) also, thus, they cannot be directly contrasted to the proposed work. Therefore, references [34] give the best results already found in this setup. Using a slightly smaller model, the work presented here surpasses it in terms of accuracy & F1-score on the SARS-Cov-2 pictures dataset. The existing model provided in Reference [34] requires 14,149,480 and 4,779,038 parameters, but the model presented here requires just 58,088,770 parameters. Training & validation loss curve results for the proposed model are 0.0204 and 0.5954for SARS-Cov-2 images; the comparison results found that the proposed model has achieved 95% precision, 93% recall, 94% F1-score and 0.94 AUC on SARS-Cov-2.

Table 11 represents the comparison results of the proposed RDD_DNN with existing state-of-art deep learning models to evaluate training & validation results of accuracy & loss. Four total models are compared, including the proposed model on the X-ray images dataset. This comparison shows that the InceptionV3 model acquired more than 90% training and testing accuracy, which is higher than ResNet. Still, it is not better than the Xception model, which has 93.49% training accuracy and 92.93% validation/testing accuracy. However, the results of InceptionV3 and Xception models were performed well by achieving more than 90% accuracy, but it was insufficient; therefore, the proposed RDD_DNN model was proposed and obtained 99.94% training accuracy and 93.97% testing accuracy, which was the top most among all models.

Table 12 represents the comparative classification results of the proposed RDD_DNN with three existing deep CNN pre-trained models [55] to compare the training and validation results in terms of precision, recall, and f1-score. These findings were compared to the X-ray images dataset. This comparison shows that the InceptionV3 model achieved 91% precision, 90% recall, and f1-score, but the ResNet model achieved 91% f1-score, 90% recall, and precision. Still, it is not well that the Xception model has 93% precision, 92% recall & f1-score. However, the results of the ResNet and Xception model were performed well by achieving more than 90% classification results, but the proposed RDD_DNN model obtained 94% precision, 91% recall, and 93% f1-score. This comparison found that the proposed model outperforms existing models in terms of precision & f1-score but the recall was not higher compared to these existing models.

From this comparative analysis, it has been summoned that the proposed model beats many existing DL models of CNN in terms of accuracy and other classification parameters for both CT scan images & X-ray images. The results of the proposed RDD_DNN model are approx. 94% Covid detection rate for X-ray images, but this detection rate was high for CT scan images of Covid, i.e., 95.10%. Thus, overall, we can say the proposed RDD_DNN model achieved 93% to 95% accuracy results for COVID-19 patients' detection.

5. Conclusions & Future Work

Our research study contributes in identification of importance of data balancing in clinical study with the experimental case study respiratory disease. It has designed and proposed an improvised image data balancing algorithm using data augmentation techniques like rotation, flipping, translation, and edge detection techniques to resolve real-time unbalanced image data in the clinical field. Also, we have contributed in proposition of improvised image enhancement and segmentation in the pre-processing of radiology pictures with the RDD_ROI technique which considers statistical correlation ship between neighbouring pixels and captures image features using GLCM. The GLCM method was used to capture feature values in a Gray-level image and texture features from the matrix and Unsupervised Learning K-mean clustering method to extract foreground and background regions. The experiments have been analysed on the two online radiology image datasets of COVID (x-ray & CT scan images) and one real time radiology image dataset for the research experimental evaluation and validation. The proposed work and experimental results focused on improving the pre-processing of radiology images to detect the spread of respiratory disease. Further, the pre-processed images are trained with our custom built RDD_DNN 28 DNN layers custom model for early detection of the spread of respiratory disease infection in human body by using machine learning approaches to benefit society.

Some future research contributions are outlines that can be further implemented to achieve a prediction model of respiratory disease:

1) Analysis and performance measure of the proposed model with existing classification models
2) Improvised prediction results in the detection of respiratory disease infection.
3) Analysis of different respiratory diseases using machine-learning techniques
4) Single technical tool in detecting respiratory disease at an early stage and benefit society.

References

[1] G. Milavetz. Global Surveillance, Prevention and Control of Chronic Respiratory Diseases: A Comprehensive Approach. Journal of Pharmacy Technology, 24(2), (2008) 122-122.

https://doi.org/10.1177/875512250802400215

[2] S.M. Levine, D.D. Marciniuk, Global Impact of Respiratory Disease: What Can We Do, Together, to Make a Difference?. Chest, 161(5), (2022) 1153–1154. https://doi.org/10.1016/j.chest.2022.01.014

[3] WHO? World Health Organization. Coronavirus disease 2019 (COVID-19) situation report, 99, 2020

[4] M.M. Rahaman, C. Li, Y. Yao, F. Kulwa, M.A. Rahman, Q. Wang, S. Qi, F. Kong, X. Zhu, X. Zhao, Identification of COVID-19 samples from chest X-Ray im-ages using deep learning: A comparison of transfer learning approaches, Journal of X-Ray Science and Technology, 28(5), (2020) 821-839. https://doi.org/10.3233/XST-200715

[5] O.E. Amani Yahiaoui, N. Yumusak, A new method of automatic recognition for tuberculosis disease diagnosis using support vector machines. Biomedical Research, 28(9), (2017) 4208-4212.

[6] Z. Hu, J. Tang, Z. Wang, K. Zhang, L. Zhang, Q. Sun, Deep learning for image-based cancer detection and diagnosis − A survey, Pattern Recognition, 83, (2018) 134–149. https://doi.org/10.1016/j.patcog.2018.05.014

[7] N.E. Dunlap, J. Bass, P. Fujiwara, P. Hopewell, C.R. Horsburgh, M. Salfinger, & P.M. Simone, Diagnostic standards and classification of tuberculosis in adults and children. American Journal of Respiratory and Critical Care Medicine, 161(4), (2000) 1376-1395.

[8] S. Sridhar, A. Kalaivani, (2021) A survey on methodologies for handling imbalance problem in multiclass classification. In Advances in Smart System Technologies: Select Proceedings of ICFSST 2019, Springer Singapore. https://doi.org/10.1007/978-981-15-5029-4_67

[9] J. Tanha, Y. Abdi, N. Samadi, Boosting methods for multi-class imbalanced data classification: an ex-perimental review. Journal of Big Data, 7(1), (2020) 1-47. https://doi.org/10.1186/s40537-020-00349-y

[10] C. Zhang, W. Tavanapong, G. Kijkul, J. Wong, P.C. De Groen, J. Oh, (2018) Similarity-based active learning for image classification under class imbalance. In 2018 IEEE international conference on data mining (ICDM), IEEE, Singapore. https://doi.org/10.1109/ICDM.2018.00196

[11] Y. Ren, X. Zhang, Y. Ma, Q. Yang, C. Wang, H. Liu, Q. Qi, Full convolutional neural network based on multi-scale feature fusion for the class imbalance remote sensing image classification. Remote Sensing, 12(21), (2020) 3547. https://doi.org/10.3390/rs12213547

[12] S. Belharbi, J. Rony, J. Dolz, Deep Interpretable Classification and Weakly-Supervised Segmentation of Histology Images via Max-Min Uncertainty. IEEE Transactions on Medical Imaging, 41(3), (2022) 702-714. https://doi.org/10.1109/TMI.2021.3123461

[13] V. Grau, A.U.J. Mewes, M. Alcañiz, R. Kikinis, S.K. Warfield, Improved Watershed Transform for Medical Image Segmentation Using Prior Information, IEEE Trans Medical Imaging, 23(3), (2018) 447-458. https://doi.org/10.1109/TMI.2004.824224

[14] R.M. Rangayyan, (2018) Biomedical Image Analysis. CRC press, United States. https://doi.org/10.1201/9780203492543

[15] R. Karthickmanoj, S. Sinthuja, N. Manoharan, Removal of impulse noise using adaptive weighted median filter. Indian Journal of Science and Technology, 7(6), (2014) 61-63.

[16] S. Lahmiri, An iterative denoising system based on Wiener filtering with application to biomedical images. Optics & Laser Technology, 90, (2017) 128-132. https://doi.org/10.1016/j.optlastec.2016.11.015

[17] A.S. Krishna, G.S. Rao, M. Sravya, Contrast enhancement techniques using histogram equalization methods on color images with poor lightning. International journal of computer science, engineering and applications, 3(4), (2013) 15-24. https://doi.org/10.5121/ijcsea.2013.3402

[18] A. Rebinth, S.M. Kumar, (2021) Wavelet Packet Transform-Based Image Classification for Computer-Aided Glaucoma Diagnosis Using Naïve Bayes Classifier. In Communication Software and Networks: Proceedings of INDIA 2019, Springer Singapore. https://doi.org/10.1007/978-981-15-5397-4_60

[19] Mahesh Kumar Jalagam, Rupalin Nanda, Rama Krushna Rath, Image Segmentation using K-means Clustering, International Journal of Advanced Science Technology, 29 (2020) 3700-3704.

[20] C Srinilta, S Kanharattanachai, (2021) Application of Natural Neighbor-based Algorithm on Oversampling SMOTE Algorithms. 2021 7th International Conference on Engineering, Applied Sciences and Technology, IEEE, Thailand. https://doi.org/10.1109/ICEAST52143.2021.9426310

[21] T. Fahrudin (2019) the Undersampling Effects on RANDSHUFF Oversampling Algorithms. 2019 4th International Conference on Information Technology, Information Systems and Electrical Engineering, IEEE, Indonesia. https://doi.org/10.1109/ICITISEE48480.2019.9003930

[22] W.U. Yuanyuan, S. Liyong, Imbalanced fuzzy

multiclass support vector machine algorithm based on class-overlap degree under sampling. Journal of University of Chinese Academy of Sciences, 35(4), (2018) 536-543. https://doi.org/10.7523/j.issn.2095-6134.2018.04.017

[23] A. Mahadevan, M. Arock, A class imbalance-aware review rating prediction using hybrid sampling and ensemble learning. Multimedia Tools and Applications, 80(5), (2021) 6911-6938. https://doi.org/10.1007/s11042-020-10024-2

[24] Wang Xiao, N. Japkowicz, Imbalanced data set learning with synthetic samples. Proc of IRIS machine learning workshop, 19(4), (2024) 420-435.

[25] T. Zhu, Y. Lin, Y. Liu, Synthetic minority oversampling technique for multiclass imbalance problems. Pattern Recognition, 72, (2017) 327-340. https://doi.org/10.1016/j.patcog.2017.07.024

[26] Y.Y. Wu, L.Y. Shen, Imbalanced Fuzzy Multiclass Support Vector Machine Algorithm Based on Class-overlap Degree Undersampling. Journal of University of Chinese Academy of Sciences, 35(4), (2018) 536-543. https://doi.org/10.7523/j.issn.2095-6134.2018.04.017

[27] B. Krawczyk, C. Bellinger, R. Corizzo, (2021) Undersampling with support vectors for multi-class imbalanced data classification. International Joint Conference on Neural Networks (IJCNN), IEEE, China. https://doi.org/10.1109/IJCNN52387.2021.9533379

[28] M.A. Arefeen, S.T. Nimi, M.S. Rahman, Neural network-based undersampling techniques. IEEE Transactions on Systems, Man, and Cybernetics: Systems, 52(2), (2020) 1111-1120. https://doi.org/10.1109/TSMC.2020.3016283

[29] Z. Xu, D. Shen, T. Nie, Y. Kou, (2020) A hybrid sampling algorithm combining M-SMOTE and ENN based on Random forest for medical imbalanced data. Journal of Biomedical Informatics, 107, 103465. https://doi.org/10.1016/j.jbi.2020.103465

[30] M. Janicka, M. Lango, J. Stefanowski, Using information on class interrelations to improve classification of multiclass imbalanced data: a new resampling algorithm. International Journal of Applied Mathematics and Computer Science, 29(4), (2019) 769-781. https://doi.org/10.2478/amcs-2019-0057

[31] S. Devaraj, M.N. Madian, (2021) Deep U-Net Network for Identifying Covid-19 Infection Using X-Ray Images, 2020 IEEE International Conference on E-health Networking, Application & Services (HEALTHCOM), China. https://doi.org/10.1109/HEALTHCOM49281.2021.9615913

[32] R. Anand, S. F. Kareem, R.M.A. Mubeen, S. Ramesh, B. Vignesh, (2021) Analysis of Heart Risk Detection in Machine Learning Using Blockchain, 6th International Conference on Signal Pro-cessing, Computing and Control (ISPCC), IEEE, India. https://doi.org/10.1109/ISPCC53510.2021.9609353

[33] X. Aggelides, A. Bardoutsos, S. Nikoletseas, N. Papadopoulos, C. Raptopoulos, P. Tzamalis, (2020) A Gesture Recognition approach to classifying Allergic Rhinitis gestures using Wrist-worn Devices : a multidisciplinary case study. 16th International Conference on Distributed Computing in Sensor Systems (DCOSS), IEEE, USA. https://doi.org/10.1109/DCOSS49796.2020.00015

[34] M.E. Chowdhury, T. Rahman, A. Khandakar, R. Mazhar, M.A. Kadir, Z.B. Mahbub, K.R. Islam, M.S. Khan, A. Iqbal, N.A. Emadi, M.B. bne Reaz, M.T. Islam, (2020) Can AI help in screening viral and COVID-19 pneumonia?. Ieee Access, 8, 132665-132676. https://doi.org/10.1109/ACCESS.2020.3010287

[35] A. Waheed, M. Goyal, D. Gupta, A. Khanna, F. Al-Turjman, P.R. Pinheiro, Covidgan: data augmentation using auxiliary classifier gan for improved COVID-19 detection. IEEE Access, 8, (2020) 91916–91923. https://doi.org/10.1109/ACCESS.2020.2994762

[36] L. Brunese, F. Mercaldo, A. Reginelli, A. Santone, Explainable deep learning for pulmonary disease and coro-navirus COVID-19 detection from x-rays. Computer Methods and Programs in Biomedicine, 196, (2020)105608. https://doi.org/10.1016/j.cmpb.2020.105608

[37] A.I. Khan, J.L. Shah, M.M. Bhat, Coronet: a deep neural network for detection and diagnosis of COVID-19 from chest x-ray image. Computer Methods and Programs in Biomedicine, 196, (2020) 105581. https://doi.org/10.1016/j.cmpb.2020.105581

[38] S. Vaid, R. Kalantar, M. Bhandari, Deep learning COVID-19 detection bias: accuracy through artificial intelligence. International Orthopaedics, 44, (2020) 1539-1542. https://doi.org/10.1007/s00264-020-04609-7

[39] A.S. Krishna, G.S. Rao, M. Sravya, Contrast enhancement techniques using histogram equalization methods on color images with poor lightning. International journal of computer science, engineering and applications, 3(4), (2013) 15. https://doi.org/10.5121/ijcsea.2013.3402

[40] S.M. Kumar, & A. Rebinth, (2020) Wavelet Packet Transform Based Image Classification for ComputerAided Glauco-ma Diagnosis Using Naïve Bayes Classifier. Communication Software

and Networks. Lecture Notes in Networks and Systems, Springer, Singapore. https://doi.org/10.1007/978-981-15-5397-4_60

[41] J.M. Kumar, R. Nanda, R.K. Rath, & G.T. Rao, Image segmentation using k-means clustering. International Journal of Advanced Science and Technology, 29, (2020) 3700-3704.

[42] M. Liu, X. Pan, S. Gao, S. Xin, Y. Zhou, (2019). Segmentation for indoor scenes based on DBSCAN clustering. Journal of Computer-Aided Design & Computer Graphics, 71(7), 1183-1193.

[43] Y. Wang, Y. Lu, Y. Li, (2019) A New Image Segmentation Method Based on Support Vector Ma-chine. IEEE 4th International Conference on Image, Vision and Computing (ICIVC), IEEE, China. https://doi.org/10.1109/ICIVC47709.2019.8981000

[44] X. Zheng, Q. Lei, R. Yao, Y. Gong, Q. Yin, Image segmentation based on adaptive K-means algorithm. EURASIP Journal on Image and Video Processing, 2018, (2018) 1-10. https://doi.org/10.1186/s13640-018-0309-3

[45] J. Chen, C. Yang, G. Xu, L. Ning, Image segmentation method using fuzzy C mean clustering based on multi-objective optimization. In Journal of Physics: Conference Series, IOP Publishing, 1004, (2018) 012035.

[46] M.L.G. Masangcap, A.M. Sison, R.P. Medina, (2018) Application of enhanced expectation maximization (EnEM) algorithm for image segmentation. In Proceedings of the 2018 International Conference on Data Science and Information Technology, 74-78. https://doi.org/10.1145/3239283.3239310

[47] S. Wazarkar, B.N. Keshavamurthy, A. Hussain, Region-based segmentation of social images using soft KNN algorithm. Procedia Computer Science, 125, (2018) 93-98. https://doi.org/10.1016/j.procs.2017.12.014

[48] J. Zhang, Z.H. Tang, W.H. Gui, Q. Chen, & J.P.Liu, (2017) Interactive image segmentation with a regression-based ensemble learning paradigm. Frontiers of Information Technology & Electronic Engineering,18(7), 1002–1020. https://doi.org/10.1631/FITEE.1601401

[49] M.Roberts, D. Driggs, M. Thorpe, J. Gilbey, M. Yeung, S. Ursprung, A.I. Aviles-Rivero, C. Etmann, C. McCague, L. Beer, J.R. Weir-McCall, Z. Teng, E. Gkrania-Klotsas, A. Covnet, J. H. F. Rudd, E. Sala, C. B. Schön-lieb. Common pitfalls and recommendations for using machine learning to detect and prognosticate for COVID-19 using chest radiographs and CT scans, Nature Machine Intelligence, 3(3), (2021) 199-217. https://doi.org/10.1038/s42256-021-00307-0

[50] P. Patel, (2020) Chest X-ray (COVID-19 & Pneumonia). Kaggle. https://www.kaggle.com/prashant268/chest-xray-covid19-pneumonia

[51] Jinyu Zhao, Yichen Zhang, Xuehai He, Pengtao Xie. (2020). COVID-19 Lung CT Scans Kaggle. https://doi.org/10.34740/KAGGLE/DS/584020

[52] E. Soares, P. Angelov, S. Biaso, M.H. Froes, D.K. Abe, (2020) SARS-CoV-2 CT-scan dataset: A large dataset of real patients CT scans for SARS-CoV-2 identification. medRxiv. https://doi.org/10.1101/2020.04.24.20078584.

[53] P. Vieira, O. Sousa, D. Magalhães, R. Rabêlo, R. Silva, Detecting pulmonary diseases using deep features in X-ray images. Pattern Recognition, 119, (2021) 108081. https://doi.org/10.1016/j.patcog.2021.108081

[54] P. Silva, E. Luz, G. Silva, G. Moreira, R. Silva, D. Lucio, D. Menotti, COVID-19 detection in CT images with deep learning: A voting-based scheme and cross-datasets analysis. Informatics in medicine unlocked, 20, (2020) 100427. https://doi.org/10.1016/j.imu.2020.100427

[55] R. Jain, M. Gupta, S. Taneja, D.J. Hemanth, Deep learning-based detection and analysis of COVID-19 on chest X-ray images. Applied Intelligence, 51, (2021) 1690–1700. https://doi.org/10.1007/s10489-020-01902-1

Authors Contribution Statement

Study conception and design: Ms. Prita Patil, Dr. Vaibhav Narawade. Data collection: Ms. Prita Patil, Dr. Vaibhav Narawade; Analysis and interpretation of results: Ms. Prita Patil, Dr. Vaibhav Narawade; Supervision: Dr. Vaibhav Narawade; Draft manuscript preparation: Ms. Prita Patil All authors reviewed the results and approved the final version of the manuscript

Funding

The authors declare that no funds, grants, or other support were received during the preparation of this manuscript.

Competing Interests

The authors declare that no competing Interest.

Data Availability

For this research, comprehensive data sourced from a Kaggle dataset has been meticulously curated and utilized as the primary foundation for analysis and experimentation.

Has this article screened for similarity?

Yes